Critical Mode Switching of Flexible-Cantilever Flutter in Low-Reynolds-Number Channel Flow

J. Cisonni[1], A. D. Lucey[1] and N. S. J. Elliott[1,2]

[1]Fluid Dynamics Research Group, Department of Mechanical Engineering
Curtin University, Perth, Western Australia, 6845, Australia

[2]Grupo de Investigación de la Dinámica de Fluidos
Xe' Lajuj No'j, Quetzaltenango, Guatemala

Abstract

Inviscid flow modelling has predominantly been employed in the numerous studies on flow-induced flutter instability of flexible cantilevers. This approach has been supported by the prevailing characteristics, giving high Reynolds numbers, of such fluid–structure interaction (FSI) systems in the wide range of engineering applications. By contrast, in this paper, a numerical model coupling a one-dimensional elastic beam model to the Navier–Stokes equations is used to determine the linear flutter-instability characteristics of a slender flexible cantilever immersed in two-dimensional viscous channel flow for laminar flow conditions. The results show that the FSI instability boundaries and the pre- and post-critical cantilever motion can be significantly altered by the non-negligible contribution of viscous effects to the hydrodynamic forces. In general, this model predicts that the FSI system becomes more stable for Reynolds numbers (based on channel height) lower than 100. For cases within this range of very low Reynolds numbers, this study focuses on the particular fluid-to-solid mass ratios at which viscous effects can possibly lead to a change in the critical mode that first becomes unstable.

Introduction

Flow-induced flutter instability of flexible cantilevers has been extensively investigated on account of the wide range of applications of this fundamental fluid–structure interaction (FSI) system. In most long-established fields of engineering where immersed flexible cantilevers are encountered, the large-scale structures and the high flow speeds give high Reynolds numbers, so inviscid flow is usually assumed in the FSI modelling [7, 5, 9]. The analysis of biomechanical systems, such as flutter of the soft palate in the upper airway during snoring [1], and the emergence of innovative energy harvesting concepts [10], have sustained interest in this canonical FSI problem. For these applications, low flow speeds or small- and micro-scale systems can give low Reynolds numbers, so the effect of viscosity on the flow-induced motion of the cantilever needs to be better understood.

To date, only limited work on the effects of viscosity on the stability of a channel-immersed cantilever has been conducted. Relatively few investigators [12, 14] have employed the Navier-Stokes equations in the modelling of this FSI system. In general, the main aim of doing so was to obtain more detailed predictions of the flow field and the vortex dynamics downstream of the cantilever free end. However, most of these studies only considered moderate Reynolds numbers ($Re \sim 10^2$) or were restricted to particular system configurations.

In this study, the FSI dynamics of a slender flexible cantilever immersed in viscous channel flow is analysed by using a numerical model coupling a one-dimensional elastic beam model to the Navier–Stokes equations. The characterisation of the linear flutter instability of the immersed cantilever for laminar flow
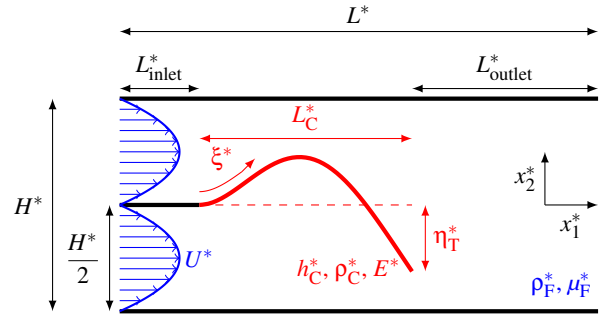

Figure 1: Description of the FSI system modelling (not to scale): flexible cantilever immersed in viscous channel flow and dimensional (indicated by an asterisk) physical quantities of the problem.

conditions shows the influence of the increased contribution of viscous effects to the hydrodynamic forces on the critical state, or flutter threshold, of the FSI system.

Theoretical Modelling

The FSI system, as shown in Fig. 1, is a flexible cantilever of length L_C^* and thickness h_C^* immersed in a viscous fluid flowing in a two-dimensional channel of length L^* and height H^* [4, 1, 2]. The fluid has density ρ_F^* and dynamic viscosity μ_F^*. The flexible cantilever has density ρ_C^* and Young's modulus E^*. It is clamped to a rigid plate of length L_{inlet}^*, parallel to the channel walls, dividing the upstream end of the channel into two inlets of identical height $H^*/2$. At both inlets, steady Poiseuille flows are imposed with average velocity U^*. At the channel outlet, located at a distance L_{outlet}^* from the downstream free end of the flexible cantilever, the flow is assumed to be parallel and axially traction-free.

The system is analysed in non-dimensional form by scaling all coordinates and lengths on H^*, velocities on U^*, fluid pressure on $\rho_F^* U^{*2}$, time on H^*/U^*, and solid tractions and stresses on the effective Young's modulus $E_{eff}^* = E^*/(1-\nu^2)$, where $\nu = 0.4$ is the Poisson ratio of the cantilever material.

The fluid flow is governed by the non-dimensional incompressible Navier–Stokes equations

$$\frac{\partial \mathbf{u}}{\partial t} + \mathbf{u} \cdot \nabla \mathbf{u} = -\nabla p + \frac{1}{Re} \nabla^2 \mathbf{u} \tag{1}$$

and the continuity equation

$$\nabla \cdot \mathbf{u} = 0 \,, \tag{2}$$

where $\mathbf{u}$ and p are, respectively, the fluid velocity and pressure, and $Re = \rho_F^* U^* H^* / \mu_F^*$ is the Reynolds number.

The flexible cantilever is chosen slender enough ($h_C^* = H^*/50$ so that $h_C^* \leq L_C^*/50$) to be assumed infinitely thin. It is modelled

as a one-dimensional elastic Kirchhoff–Love beam, allowing for geometric non-linearity. Its undeformed shape is parameterised by a single Lagrangian coordinate ξ, so that the position vector to a material point on the cantilever's centreline in the undeformed configuration is given by $\mathbf{r}_c(\xi)$. The solid deformation due to an applied traction $\mathbf{T}_{\text{eff}}$ causes the material points on the cantilever's centreline to be displaced to their new positions $\mathbf{R}_c(\xi)$. The cantilever deformation is then governed by the principle of virtual displacements (PVD) given by

$$\int_0^{L_C} \left\{ \gamma\delta\gamma + \frac{h_C^2}{12}\kappa\delta\kappa - \left(\frac{1}{h_C}\sqrt{\frac{A}{a}}\mathbf{T}_{\text{eff}} \right.\right.$$
$$\left.\left. - \frac{Ca_{\text{eff}}}{Mh_L}\frac{\partial^2\mathbf{R}_c}{\partial t^2} \right) \cdot \delta\mathbf{R}_c \right\}\sqrt{a}\,d\xi = 0, \quad (3)$$

where

$$a = \frac{\partial\mathbf{r}_c}{\partial\xi}\cdot\frac{\partial\mathbf{r}_c}{\partial\xi}, \quad A = \frac{\partial\mathbf{R}_c}{\partial\xi}\cdot\frac{\partial\mathbf{R}_c}{\partial\xi}, \quad (4a,b)$$

are the squares of the lengths of infinitesimal material line elements in the undeformed and deformed configurations, respectively. Therefore, the ratio $\sqrt{A/a}$ represents the stretch of the cantilever centreline while the strain γ and bending κ are given by

$$\gamma = \frac{1}{2}(A-a), \quad \kappa = -(C-c), \quad (5a,b)$$

with

$$c = \mathbf{n}_c\cdot\frac{\partial^2\mathbf{r}_c}{\partial\xi^2}, \quad C = \mathbf{N}_c\cdot\frac{\partial^2\mathbf{R}_c}{\partial\xi^2}, \quad (6a,b)$$

representing the curvature of the cantilever centreline, respectively, before and after the deformation. $\mathbf{n}_c$ and $\mathbf{N}_c$ denote the unit normals (pointing into the fluid) to the top face of the undeformed and deformed cantilever centreline, respectively. The effective Cauchy number

$$Ca_{\text{eff}} = \frac{\rho_F^* U^{*2}}{E_{\text{eff}}^*} = \frac{MU^2 h_L^3}{12} \quad (7)$$

represents the ratio between the fluid inertial forces and the solid elastic forces, where

$$M = \frac{\rho_F^* L_C^*}{\rho_C^* h_C^*}, \quad h_L = \frac{h_C^*}{L_C^*}, \quad U = U^* L_C^*\sqrt{\frac{\rho_C^* h_C^*}{B^*}}, \quad (8)$$

are, respectively, the mass ratio, the cantilever thickness-to-length ratio and the reduced velocity, with the flexural rigidity $B^* = E_{\text{eff}}^* h_C^{*3}/12$.

When the flexible cantilever is immersed in the channel flow, the fluid traction that acts on the cantilever centreline, combining the fluid tractions acting on its top and bottom faces, depends on the pressure and viscous shear stress, so that

$$\mathbf{T}_{\text{eff}} = Ca_{\text{eff}} \left\{ \left(p|_{\text{top}}\,\mathbf{I} - \frac{1}{Re}\left(\nabla\mathbf{u}+(\nabla\mathbf{u})^{\text{T}}\right)\Big|_{\text{top}} \right)\cdot\mathbf{N}_c \right.$$
$$\left. - \left(p|_{\text{bottom}}\,\mathbf{I} - \frac{1}{Re}\left(\nabla\mathbf{u}+(\nabla\mathbf{u})^{\text{T}}\right)\Big|_{\text{bottom}} \right)\cdot\mathbf{N}_c \right\}. \quad (9)$$

For small deformations of the flexible cantilever and inviscid flow, a solution for the PVD given in Eq. (3) is of the form of the well known pressure-driven *Euler–Bernoulli* beam equation

$$\frac{\partial^2\eta}{\partial t^2} + \frac{L_H^2}{U^2}\frac{\partial^4\eta}{\partial x_1^4} = \frac{M}{L_H}\Delta p, \quad (10)$$

where $\eta(x_1)$ is the vertical deflection of the cantilever centreline in the Eulerian coordinate system, $\Delta p(x_1)$ is the distributed pressure difference between the top and bottom faces of the cantilever, and $L_H = L_C = L_C^*/H^*$ is the ratio between cantilever length and channel height. This simplified formulation of the cantilever dynamics, used in numerous studies [7, 3, 9], provides a useful reference to the *in vacuo* analytical solution (i.e. $\Delta p = 0$).

Computational Methods

The problem was formulated using the open-source finite-element library oomph-lib [8]. The flexible cantilever was spatially discretised using two-node Hermite beam elements and the fluid domain using nine-node quadrilateral Taylor–Hood elements with adaptive mesh refinement capabilities. Time stepping was done with a Newmark scheme for the solid and a second-order backward differentiation formula scheme for the fluid. The FSI problem was discretised monolithically and the Newton–Raphson method was used to solve the non-linear system of equations, employing the SuperLU direct linear solver within the Newton iteration.

The analysis of the stability/instability of the FSI system was carried out for variations of the four main non-dimensional parameters, M, U, L_H and Re. The main numerical experiments consisted in running time-marching simulations of the FSI system to obtain the properties of the flexible cantilever oscillations over the whole (M,U) domain considered for different combinations of (L_H, Re). It is noted that variations of the non-dimensional reduced velocity U for a constant Reynolds number Re correspond to variations of the cantilever flexural rigidity B^* while keeping the dimensional flow velocity U^* constant. For each simulation, the initialisation procedure involved:

1. prescribing the deformation of the cantilever into the second in vacuo eigenmode with small (linear mechanics) amplitude under no-flow conditions;
2. constraining the cantilever in position;
3. gradually introducing the flow in a sequence of steady states; and
4. releasing the cantilever and solving the unsteady FSI problem.

The linear stability or instability of the FSI system was determined from the time trace of the simulated deflection of the flexible cantilever tip η_T, as shown in Fig. 1. The dimensional exponential growth rate α_T^* and frequency f_T^* of the cantilever tip oscillations were used to estimate the normalised exponential growth rate $\alpha_T = \alpha_T^*/f_T^*$, corresponding to the strength of the instability or instability.

Results

Consolidation of the data obtained from the numerical experiments provides a detailed characterisation of the dynamics of the immersed flexible cantilever in the (M, U) parameter space for fixed L_H and Re. Figures 2(a) and 3(a) show the exponential growth/decay rate α_T of the amplitude of the oscillatory motion of the cantilever tip for $Re = 200$ and $Re = 20$, respectively. The strength of stability ($\alpha_T < 0$) or instability ($\alpha_T > 0$) is represented by the magnitude of α_T, designated by marked contours. The neutral stability, demarcating the boundary between stable and unstable oscillations, is represented by the thick solid line corresponding to $\alpha_T = 0$. This curve shows the effect of the mass ratio M on the critical reduced velocity U_{crit} required to destabilise the flexible cantilever. It highlights the complex interactions of the flow with the different structural modes; the sequence of lobes indicating mode-switching from lower to higher order with increasing M. This classical shape, with several modal branches, has been seen in many previous studies, e.g. [5, 13], including those that assume an inviscid
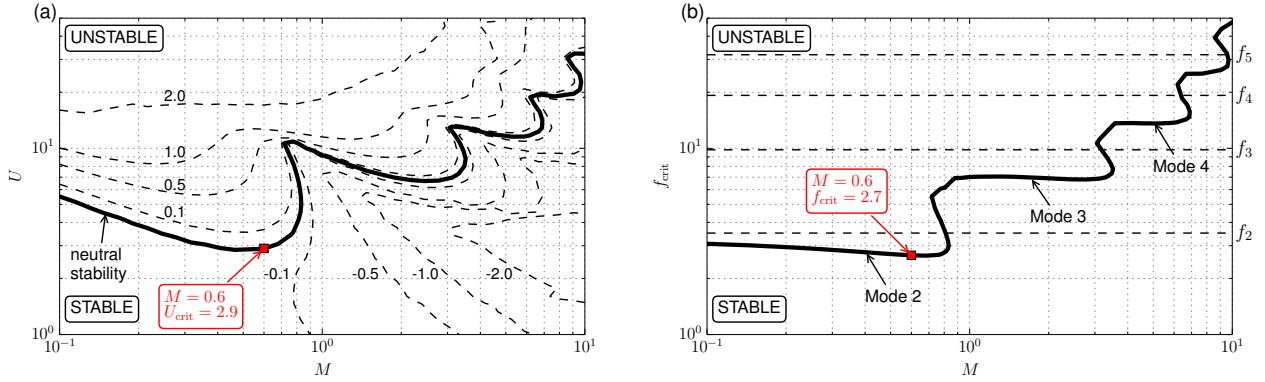
Figure 2: Dynamic characteristics of the immersed flexible cantilever for $L_H = 2$ and $Re = 200$: (a) Contours of the exponential growth rate α_T as functions of mass ratio M and reduced flow velocity U. The thick solid line corresponds to neutral stability ($\alpha_T=0$). (b) Oscillation frequency of the cantilever motion at neutral stability f_{crit} as a function of mass ratio M. The cantilever eigenfrequencies (*in vacuo* linear theory) associated with Modes 2 to 5 are indicated with dashed lines.
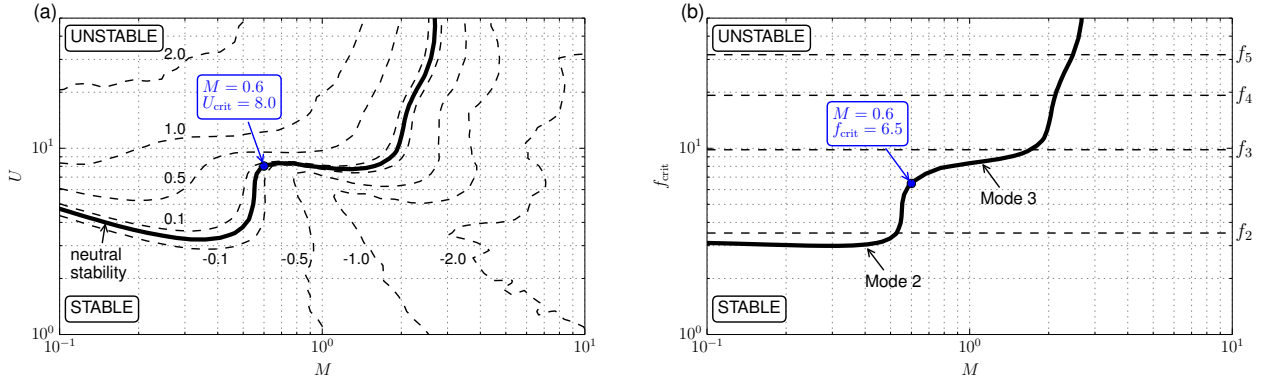

Figure 3: Dynamic characteristics of the immersed flexible cantilever for $L_H = 2$ and $Re = 20$: (a) Contours of the exponential growth rate α_T as functions of mass ratio M and reduced flow velocity U. The thick solid line corresponds to neutral stability ($\alpha_T=0$). (b) Oscillation frequency of the cantilever motion at neutral stability f_{crit} as a function of mass ratio M. The cantilever eigenfrequencies (*in vacuo* linear theory) associated with Modes 2 to 5 are indicated with dashed lines.

fluid. Figures 2(b) and 3(b) show the effect of the mass ratio M on the critical frequency f_{crit}, at which the cantilever tip oscillates when the system is neutrally stable ($U = U_{crit}$). For all mode orders, the immersed cantilever oscillates at a frequency lower than the *in vacuo* linear eigenfrequency associated with the corresponding structural mode. The lower frequency values can be linked to observations from earlier studies [6, 11], in which fluid-inertia loading causes a decrease, primarily dependent upon the mass ratio, of the oscillation frequency of a structure in a fluid, compared with the *in vacuo* case.

In contrast to the many studies that assume inviscid flow, hence infinite Reynolds number, the present stability analysis uses unsteady laminar flow. The comparison between data shown in Figs. 2 and 3 provides an indication of the effects of viscosity on the cantilever dynamics, and more particularly on the critical velocities and frequencies. For a drop in Reynolds number by one order of magnitude, the neutral stability curves globally retain their main features. However, when compared to the $Re = 200$ curves, the modal transitions for $Re = 20$ are less abrupt, and all the structural modes of order greater than 3 are strongly stabilised and do not become the dominant response within the range of reduced velocities considered. Also, the critical velocity curve is shifted to lower mass ratios, so that the transition from Mode 2 to Mode 3 is triggered for a lower value of M. Thus, the increased contribution of the viscous effects to

the hydrodynamic forces exerted by the axial flow on the cantilever can result in an increase in the critical frequency for a given mass ratio.

With an inviscid FSI model, the predictions of U_{crit}, f_{crit} and the first unstable structural mode would only be determined by the value of mass ratio. By contrast, with the present FSI model, for the illustrative mass ratio $M = 0.6$, the critical velocity changes from $U_{crit} = 2.9$ at $Re = 200$ to $U_{crit} = 8.0$ at $Re = 20$, as indicated in Figs. 2 and 3. By more than doubling the critical velocity value, viscous effects produce, in this case, a significant stabilisation of the FSI system. More importantly, while Mode 2 is the first unstable structural mode at $Re = 200$, Mode 3 becomes the first unstable structural mode at $Re = 20$. Consequently, the critical frequency also more than doubles when the Reynolds number decreases from 200 ($f_{crit} = 2.7$) to 20 ($f_{crit} = 6.5$). Figure 4 shows the strength of stability/instability in the (Re,U) parameter space and the effect of the Reynolds number on the critical velocity and frequency curves for $M = 0.6$. The trajectories in the (Re,U) parameter space correspond to two cases involving fluids having different density ρ_F^* and viscosity μ_F^*, while keeping the other dimensional geometric and material properties of the system constant. These two trajectories represent the variations of the Reynolds number and the reduced velocity with the variation of the dimensional flow velocity U^*. It can be seen that they cross the neutral stability curve in two different loca-
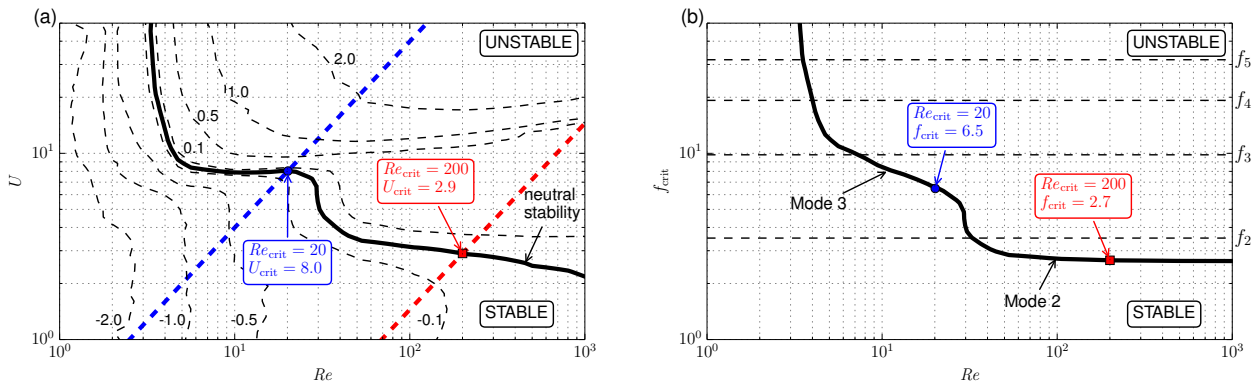
Figure 4: Dynamic characteristics of the immersed flexible cantilever for $L_H = 2$ and $M = 0.6$: (a) Contours of the exponential growth rate α_T as functions of Reynolds number Re and reduced flow velocity U. The thick solid line corresponds to neutral stability (α_T=0). (b) Oscillation frequency of the cantilever motion at neutral stability f_{crit} as a function of Reynolds number Re. The cantilever eigenfrequencies (*in vacuo* linear theory) associated with Modes 2 to 5 are indicated with dashed lines.

tions. This leads to substantially different predicted conditions of the critical state for the two cases.

Conclusions

A numerical model has been employed to characterise the dynamics of a flexible cantilever immersed in viscous channel flow. In general, it is shown that a decrease in Reynolds number does not fundamentally modify the FSI mechanism but has a stabilising effect on the system, in particular for high fluid-to-solid mass ratios. Large variations of the neutral stability characteristics and a possible change in the first unstable structural mode can arise from more dominant viscous effects within the flow.

Acknowledgements

References

[1] Cisonni, J., Elliott, N.S.J., Lucey, A.D. and Heil, M., A compound cantilevered plate model of the palate-uvula system during snoring, *Proceedings of the 19th Australasian Fluid Mechanics Conference*, 2014.

[2] Cisonni, J., Lucey, A.D. and Elliott, N.S.J., Stability of a cantilevered flexible plate with non-uniform thickness in viscous channel flow, *Proceedings of the 3rd Symposium on Fluid-Structure-Sound Interactions and Control*, editors Zhou, Y., Lucey, A.D., Liu, Y. and Huang, L., Springer, 2016, 333–337.

[3] Doaré, O., Suazade, M. and Eloy, C., Flutter of an elastic plate in a channel flow: Confinement and finite-size effects, *J. Fluid. Struct.*, **27**, 2011, 76–88.

[4] Elliott, N.S.J., Lucey, A.D. and Heil, M., Large-amplitude oscillations of a finite-thickness cantilevered flexible plate in viscous channel flow, *Proceedings of the 3rd Joint US-European Fluids Engineering Summer Meeting and 8th International Conference on Nanochannels, Microchannels and Minichannels*, 2010.

[5] Eloy, C., Lagrange, R., Souilliez, C. and Schouveiler, L., Aeroelastic instability of cantilevered flexible plates in uniform flow, *J. Fluid. Mech.*, **611**, 2008, 97–106.

[6] Fu, Y. and Price, W.G., Interactions between a partially or totally immersed vibrating cantilever plate and the surrounding fluid, *J. Sound Vib.*, **118**, 1987, 495–513.

[7] Guo, C.Q. and Païdoussis, M.P., Stability of rectangular plates with free side-edges in two-dimensional inviscid channel flow, *J. Appl. Mech.*, **67**, 2000, 171–176.

[8] Heil, M. and Hazel, A.L., oomph-lib — an Object-Oriented Multi-Physics Finite-Element Library, *Fluid-Structure Interaction*, editors Schäfer, M. and Bungartz, H.-J., Springer, 2006, 19–49.

[9] Howell, R.M., Lucey, A.D., Carpenter, P.W. and Pitman, M.W., Interaction between a cantilevered-free flexible plate and ideal flow, *J. Fluid. Struct.*, **25**, 2009, 544–566.

[10] Howell, R.M. and Lucey, A.D., Flutter of spring-mounted flexible plates in uniform flow, *J. Fluid Struct.*, **59**, 2015, 370–393.

[11] Shabani, R., Hatami, H., Golzar, F.G., Tariverdilo, S. and Rezazadeh, G., Coupled vibration of a cantilever micro-beam submerged in a bounded incompressible fluid domain, *Acta Mech.*, **224**, 2013, 881–850.

[12] Shoele, K. and Mittal, R., Computational study of flow-induced vibration of a reed in a channel and effect on convective heat transfer, *Phys. Fluids*, **26**, 2014.

[13] Shoele, K. and Mittal, R., Flutter instability of a thin flexible plate in a channel, *J. Fluid. Mech.*, **786**, 2016, 29–46.

[14] Watanabe, Y., Isogai, K,. Suzuki, S. and Sugihara, M., A Theoretical study of paper flutter, *J. Fluid. Struct.*, **16**, 2002, 543–560.